Uludağ University Journal of The Faculty of Engineering, Vol. 27, No. 3, 2022 RESEARCH

DOI: 10.17482/uumfd.1121360

DYNAMIC MODELING AND CONTROL OF AN ELECTRO-MECHANICAL FIN LOADING SYSTEM

Bülent ÖZKAN*

Received: 25.05.2022; revised: 11.08.2022; accepted: 01.09.2022

Abstract: In this study, the design of an electro-mechanical fin loading system which is utilized to simulate the effects of the aerodynamic moment occurring in an atmospheric flight on a missile system is dealt with. In this extent, the dynamic modeling of the dedicated loading system is constructed and then the control system is designed on that model. As the control algorithm, the classical control system operating with regard of the PID (proportional plus integral plus derivative) control action and the robust control system designed according to the H_∞ norm are taken into consideration. Once the mentioned control systems are built, the relevant computer simulations are performed with the inclusion of a realistic control actuation system model in accordance with the consistent numerical values of the necessary parameters. As a result of this work, it is observed that the robust control system yields more satisfactory results than its classical counterpart even under more severe conditions.

Keywords: Fin loading system, classical control, robust control, aerodynamic load, control actuation system

Elektromekanik Eyletimli Bir Kanat Yükleme Cihazının Dinamik Modellemesi ve Denetimi

Öz: Bu çalışmada, atmosfer içerisinde uçan bir füzeye etkiyen aerodinamik moment etkisinin yerde benzetimini yapmak amacıyla tasarlanan elektromekanik eyletimli bir kanat yükleme cihazının tasarımı ele alınmaktadır. Bu kapsamda, göz önüne alınan kanat yükleme cihazının dinamik modeli çıkarılmış ve ardından bu model üzerine denetim sistemi tasarlanmıştır. Denetim sistemi olarak, PID (oransal, tümlevsel ve türevsel) denetim işlemini esas alan klasik denetim sistemi ile H_∞ normunu esas alarak sentezlenen gürbüz denetim sistemi uygulanmıştır. Denetim sistemi oluşturulduktan sonra, ilgili parametreler için belirlenen tutarlı sayısal değerler kullanılarak modellenen gerçekçi bir kontrol tahrik sistemi de toplam sistem şemasına dahil edilerek bilgisayar benzetimleri gerçekleştirilmiştir. Benzetimler sonucunda, çok daha zorlu işletim koşulları altında dahi gürbüz denetim sisteminin klasik denetim sistemine nazaran daha tatminkâr çıktılar ürettiği gözlenmiştir.

Anahtar Kelimeler: Kanat yükleme cihazı, klasik denetim, gürbüz denetim, aerodinamik yük, kontrol tahrik sistemi

1. INTRODUCTION

One of the most important subsystems of the guided missiles is the control actuation system (CAS) in the sense of orienting them towards predetermined targets at a desired accuracy level (Arulmozhiyal et al., 2015). In practical applications, the CAS which is responsible of converting the command signals generated by the missile control system into reasonable physical motion by means of the control fins is subjected to the disturbing moments originated from aerodynamic effects (Muniraj and Arulmozhiyal, 2015). These effects are in general called “hinge moment effects”. Actually, the hinge moment may change its direction and magnitude depending on the

* Gazi Üniversitesi Mühendislik Fakültesi Eti Mah. Yükseliş Sok. No: 5, 06570, Çankaya, Ankara, TURKEY, e-mail: bozkan37@gmail.com

speed, altitude, angle of attack, and angular positions of the control fins of the relevant munition. Therefore, it is necessary to evaluate the effects of the hinge moment on the CAS in order to estimate the behavior of the CAS in a realistic implementation (Nam et al., 2000).

In order to simulate the hinge moment effects on a CAS, the design of a convenient fin loading system (FLS) comes into the picture. In such systems, the force or torque quantity that will be applied to the CAS is selected as the control variable while the angular position of the CAS is taken as an external input on the dedicated control system. The FLS setups are widely used in aerospace industries so as to fulfill the mentioned functions (Blasi et al., 2021; Borrelli at al., 2020).

In the construction of an FLS as stated above, accuracy constitutes one of the important issues. Moreover, the robustness of the control system against disturbing effects such as mechanical vibrations and sensor noises should also be taken into account. For this purpose, the robust control methods including backstepping and sliding mode control are applied on aerodynamic fin loading systems (Özakalın et al., 2014; Özkan, 2017). Regarding the factors mentioned above as well as the compactness of the resulting structure, the electro-mechanical FLS becomes superior to its electro-hydraulic and pneumatic counterparts. An example to the electro-mechanical FLS can be given as in Figure 1 (Maekawa, 1999; Tekin and Şahin, 2008).

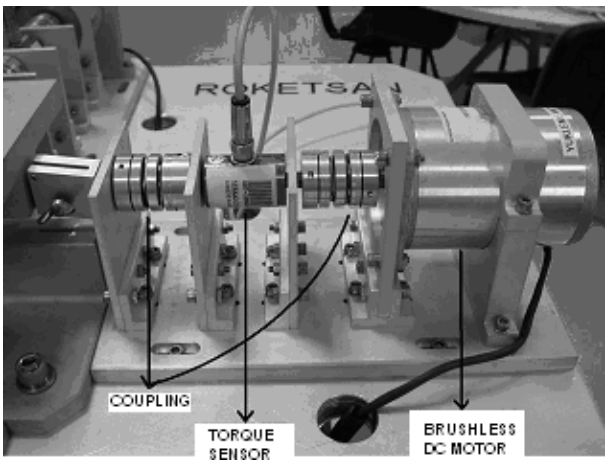

Figure 1:
Electro-mechanical type fin loading system <(Tekin and Şahin, 2008)>

On the other hand, the electro-hydraulic ones gain more importance when the force or torque requirements become larger. Especially when the duration of force or torque application at large amount is considered, the electro-hydraulic mechanisms are preferably designed because of their ability on working properly without facing with any heating problem for a long time (http://www.ideal-aerosmith.com/images/aerofinloader_large.jpg; Jing et al., 2019; Page and Willis, 1998). However, the nonlinear dynamical behavior of hydraulic systems makes the design of electro-hydraulic mechanisms more difficult and hence the electro-mechanical loading systems are chosen in most of the practical applications provided that the force or torque requirement is smaller. The solid model view of an electro-hydraulic loading system with hydraulic motors at appropriate sizes is shown in Figure 2 (Tekin and Şahin, 2008).

In this study, an electro-mechanical FLS which is intended to be used to exert the pre-calculated aerodynamic moments on an electro-mechanical CAS is dealt with. First, the dynamic model of the proposed system is derived. Based on the resulting equations, the corresponding control system is designed with classical and robust controllers. The PID (proportional plus integral plus derivative) action is employed in the classical control system scheme while the robust controller is synthesized according to the H_∞ norm. In both types of the control systems,

the angular deflections of the rods connecting the control fins to the relevant actuators of the CAS are assumed as external disturbances on the FLS at reasonable levels. Also, the control architecture of the CAS is constructed based on a robust controller with respect to the H_∞ norm. As the main contribution of this work, it is demonstrated that the robust control scheme yields more satisfactory results for the designated performance parameters in the sense of torque control than the classical methods.

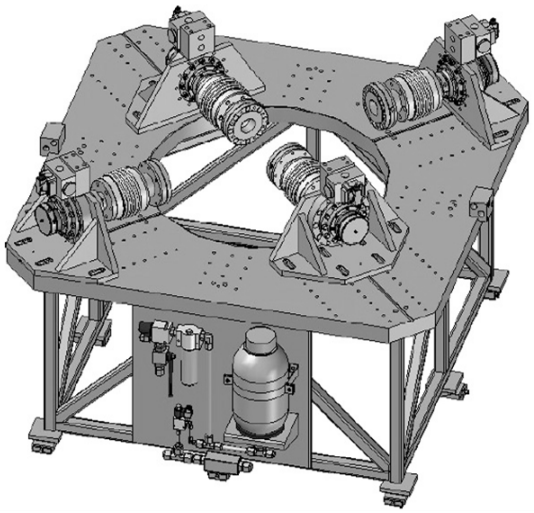

Figure 2:
Hydraulic motor type fin loading system
<(https://www.ideal-aerosmith.com/ideal-product/aeroload-simulation-system)>

2. DYNAMIC MODELING OF THE FIN LOADING SYSTEM

The FLS should be able to excite as many of the fin connecting rods of a CAS as desired. In this sense, it seems more advantageous to design the system in a modular manner. Thus, a single-axis electro-mechanical FLS can be built as schematized in Figure 3.

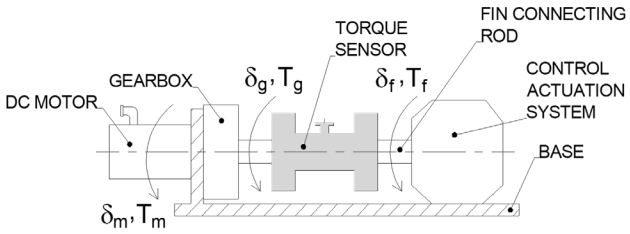

Figure 3:
Single axis fin loading system

The proposed structure is composed of a brushless DC electric motor, a gearbox, a torque sensor, and a fin connecting rod between the FLS and CAS as seen in Figure 3. Here, δ_m, δ_g, and δ_f stand for the angular position variables of the motor output shaft, gearbox output shaft, and fin connection rod, respectively while T_m, T_g, and T_f denote the torque quantities on the listed components. The measurement of the torque value on the gearbox output shaft is performed by means of strain gauge set at the mid-point of the torque sensor.

As N indicates the reduction ratio of the gearbox ($N>1$), the position and torque variables of the motor and gearbox output shafts can be related to each other as follows:

$$\delta_g = \delta_m / N \tag{1}$$

$$T_g = N T_m \tag{2}$$

The output torque of the motor is generated proportional to the current command (I) in accordance with the corresponding motor torque constant (K_t) as given below:

$$T_m = K_t I \tag{3}$$

Representing the equivalent moment of inertia of the DC motor, gearbox components, and half-portion of the torque sensor from the connection point with the gearbox shaft to the location of the strain gauge set as J_e and calling the equivalent viscous friction coefficient B_e, the dynamics of the FLS reduced on the gearbox output shaft can be written in the following manner:

$$J_e \ddot{\delta}_g + B_e \dot{\delta}_g + K_s \left(\delta_g - \delta_f\right) = T_g \tag{4}$$

where K_s shows the torque sensor gain.

3. CONTROL SYSTEM DESIGN

In order to apply the control torques to the fin connection rods of the CAS in a controllable manner, the control system of the FLS is designed in two different schemes. First, the classical PID type control algorithm is constructed. Afterwards, a robust control system is built according to the H_∞ norm to suppress the undesired effects of the disturbing torques and sensor noises on the system (Ogata, 1997).

In order to simulate their performances in the physical world as realistic as possible, the designed control systems in the continuous-domain should be converted into the discrete-domain-systems. After expressing the controller transfer functions in the state space, the resulting matrices are then turned into discrete domain matrices via the appropriate MATLAB® commands. In the mentioned conversion, the sampling frequency is selected to be 40 times the desired bandwidth value of the control systems so as to guarantee the control stability. Hence, the continuous controller model can be discretized using the Euler's method as follows (Low et al., 2005):

$$x(n+1) = A_d\, x(n) + B_d\, u(n) \tag{5}$$

$$y(n) = C_d\, x(n) + D_d\, u(n) \tag{6}$$

where x and y denote the state variables and controller output while A_d, B_d, C_d, and D_d stand for the discrete-time system, input, output, and disturbance matrices. Also, "n" indicates the step-size used in the calculation.

3.1. Classical Control System

Based on the FLS dynamics given in (4), a classical torque control system can be established with regard of the PID control action as shown in the block diagram in Figure 4.

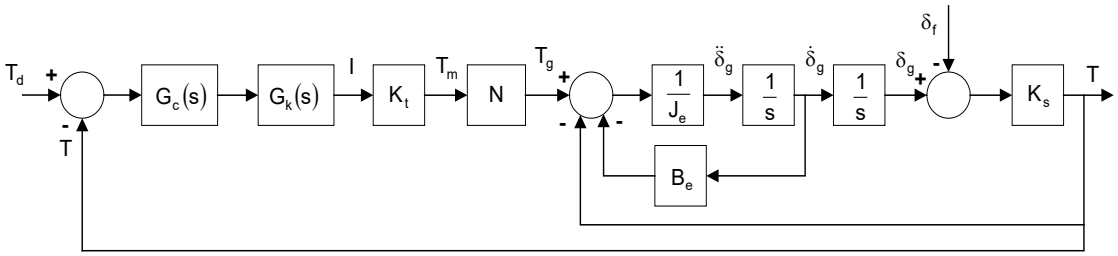

Figure 4:
Torque control system with the classical controller

In Figure 4, T_d and T represent the desired and actual values of the torque applied to the fin connecting rod. Also, $G_c(s)$ and $G_k(s)$ are the transfer functions of the controller and driver unit where "*s*" stands for the Laplace operator. Since the operating frequency of the driver unit is much greater than the desired bandwidth of the entire control system, $G_k(s)$ can be assumed as unity. Also, $G_c(s)$ can be expressed in terms of the proportional, integral, and derivative gains (K_p, K_i, and K_d) of the PID type controller in the following fashion:

$$G_c(s) = K_p + K_i / s + K_d\, s \tag{7}$$

Simplifying the scheme in Figure 4 using the block diagram algebra, the actual torque quantity (T) can be obtained in terms of T_d and δ_f with the insertion of the transfer functions from T to T_d [$G_{T_dT}(s)$] and T to δ_f [$G_{\delta_f T}(s)$] as follows:

$$T(s) = G_{T_dT}(s)T_d(s) - G_{\delta_f T}(s)\delta_f(s) \tag{8}$$

In (8), the expanded forms of $G_{T_dT}(s)$ and $G_{\delta_f T}(s)$ are as given below:

$$G_{T_dT}(s) = \frac{n_{T2}\, s^2 + n_{T1}\, s + 1}{d_3\, s^3 + d_2\, s^2 + d_1\, s + 1} \tag{9}$$

$$G_{\delta_f T}(s) = \frac{s^2\left(n_{\delta 1}\, s + n_{\delta 0}\right)}{d_3\, s^3 + d_2\, s^2 + d_1\, s + 1} \tag{10}$$

where, for $\mu = N K_t K_i$, $n_{T1} = K_p / K_i$, $n_{T2} = K_d / K_i$, $n_{\delta 0} = B_e / \mu$, $n_{\delta 1} = J_e / \mu$, $d_1 = \left(1 + N K_t K_p\right)/\mu$, $d_2 = \left(B_e / K_s + N K_t K_p\right)/\mu$, and $d_3 = J_e /\left(\mu K_s\right)$.

The controller gains can be determined by placing the poles of the closed loop control system to suitable locations so as to have the desired bandwidth value. In the pole placement, the use of the Butterworth polynomials is one of the frequently-used methods. Here, the third-order Butterworth polynomial taking the damping ratio as 0.7 is as given below (Özkan, 2005):

$$B_3(s) = \frac{s^3}{\omega_c^3} + \frac{2s^2}{\omega_c^2} + \frac{2s}{\omega_c} + 1 \tag{11}$$

Thus, equating the characteristic polynomial of the proposed control system, i.e. the denominator polynomials of $G_{T_d T}(s)$ and $G_{\delta_f T}(s)$, to (11), K_p, K_i, and K_d happen to be as follows:

$$K_p = \left(2 J_e \omega_c^2 - K_s\right)/\left(N K_t K_s\right) \tag{12}$$

$$K_i = J_e \omega_c^3 /\left(N K_t K_s\right) \tag{13}$$

$$K_d = \left(2 J_e \omega_c - B_e\right)/\left(N K_t K_s\right) \tag{14}$$

3.2. Robust Control System

In order to overcome the undesired effects of the disturbances on the system, a robust controller is designed with respect to the H_∞ norm using the control toolbox of the MATLAB® (Özkan et al., 2008). The block diagram of the dedicated control system is given in Figure 5, and the relevant inputs and outputs of the controller are shown given in Figure 6.

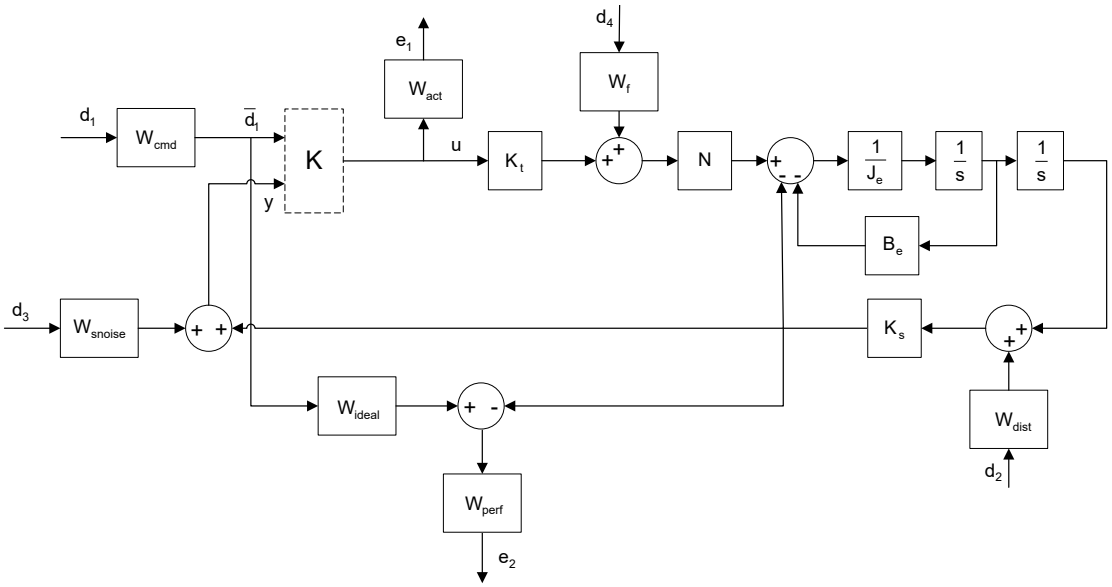

Figure 5:
Torque control system with the robust controller

In this scheme, d_1, d_2, d_3, and d_4 stand for the command signal of the control system, angular displacement of the control actuation system, noise on the torque mearument, and nonlinear frictional effect, respectively. The corresponding weightings are shown as W_{cmd}, W_{dist}, W_{snoise}, and W_f. Here, W_{cmd} is designated as a low pass filter with the maximum value of 60 N·m and corner frequency of 4 Hz in order to limit the torque command at these torque and frequency values. Another low pass filter having the maximum value of 1° and corner frequency of 3 Hz is assigned to W_{dist}. Depending on the estimation of the maximum amount of the noise on the torque measurement, W_{snoise} is assumed as 0.225 N·m to be a constant number. Also, it is regarded that W_f =0.6 N·m in a similar fashion. Regarding these selections, W_{snoise} and W_f are assigned to be valid along the whole frequency range up to the chosen f_c value.

In the proposed control system, the controller (K) is designed to minimize e_1 and e_2 which denote the penalties of the control signal and deviation from the ideal system. Furthermore, y and u represent the input and output of the controller. As W_{act} is designated as 1/15 A^{-1} regarding that the maximum current consumption becomes at an amount of 15 A, W_{perf} is decided to be 1/0.5

$(N \cdot m)^{-1}$. In the selection of the weighting function W_{perf}, it is considered that the maximum deviation of the designed control system from the ideal system be 0.5 N·m.

Finally, the ideal system desired to be reached with the designed robust control system is described by the following transfer function:

$$w_{ideal} = \omega_n^2 / \left(s^2 + 2\zeta\,\omega_n\, s + \omega_n^2 \right) \tag{15}$$

where ω_n and ζ represent the natural frequency and damping ratio specified for the ideal control system, and it is taken that $\omega_n = 2 \cdot \pi \cdot 40$ rad/s (=40 Hz) and ζ=0.7 (critical damping).

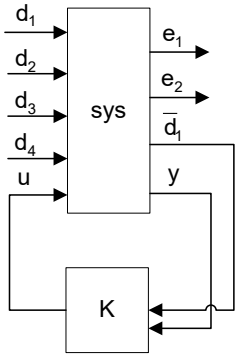

Figure 6:
Robust control system model

Regarding the designations and selections above, K appears to be a sixth-order transfer function.

4. COMPUTER SIMULATIONS

In order to observe the performance characteristics of the proposed control systems, the FLS and CAS models are established in the MATLAB® Simulink® environment. As both the classical and robust control systems are considered for the FLS, the CAS is assumed as an electro-mechanical type robust control system obeying the H_∞ norm. For the parameters of the mentioned models, the numerical values given in Table 1 are taken into account.

Table 1. Numerical values used in the computer simulations

Parameter	Aerodynamic Fin Loader	Control Actuation System
K_t (N·m/A)	0.60	0.45
N	40	55
J_e (kg·m^2)	0.50	0.30
B_e (N·m·s/rad)	0.85	0.02
K_s (N·m/rad)	3.3×10^4	-
f_c (Hz)	40	10
Simulation Sampling Frequency (Hz)	2000	

Using these models, the relevant computer simulations are conducted in discrete mode. Here, the gains of the PID type controller of the FLS are calculated to be K_p=0.055, K_i=10.022, K_d=3.82×10^{-4}. Also, the transfer functions between the filtered reference input and the controller

output [$G_d(s)$] and between the actual output and controller output [$G_y(s)$] are determined in the following manner:

$$G_d(s)=\frac{8.7s^6+2.5s^5+2.2s^4+6.6s^3+6.7s^2+9.4s+1.6\times10^{24}}{s^7+1.2s^6+3.9s^5+4.9s^4+1.2s^3+3.9s^2+6.8s+1.2\times10^{25}} \quad (16)$$

$$G_y(s)=\frac{2.5s^5+3.9s^4+1.8s^3+4.1s^2+2.9s+4.3\times10^{20}}{s^6+1.2s^5+3.6s^4+3.9s^3+1.5s^2+2.7s+4.6\times10^{21}} \quad (17)$$

In the simulations, the reference (desired) torque input of the FLS is designated as a sine function in the form of $T_d = T_{d0} \cdot sin(2 \cdot \pi \cdot f_d)$ while the CAS is subjected a sinusoidal input as $\delta_f = \delta_{f0} \cdot sin(2 \cdot \pi \cdot f_d)$. Setting T_{d0}=60 N·m and f_d=5 Hz in all the simulations, the values of 1 and 3° are assigned to δ_{f0} in order to see the effectiveness of the control systems against different fin deflection values. Furthermore, the FLS is thought to be affected by a torque sensor noise with a maximum amount of 0.15 N·m and a noise with the maximum value of 2×10^{-4} rad is put on the angular position sensor of the CAS. Also, the current limits of the FLS and CAS are set to 15 and 5 A, respectively.

Hence, running the constructed models in the MATLAB® environment with regard of the parameter values given above, the graphs are obtained for the desired and actual values of the fin deflections and hinge moments as well as the current consumption plots regarding both the 1 and 3° fin deflection amplitudes as given Figure 7 through Figure 16. Moreover, the attained numerical results are given in Table 2. In order to show the responses of the proposed control systems clearly, the first 0.3 s of the simulations are viewed in the graphs.

For the cases with δ_{f0}=1°, the maximum current consumption values are obtained as 1.91 and 4.16 A for PID and H_∞ type FLS controllers, as shown in Figure 9 and Figure 12, respectively. This means that the robust control system requires more current in order to compensate the undesired effects of the disturbing inputs on the system. These quantities become as 2.49 and 4.52 A for δ_{f0}=3° indeed. Actually, it is seen that the current consumption of both the control systems decrease in contrast to the increment in the magnitude of the fin deflection. This implies that there is no direct relationship between the desired deflection values of the CAS fins and the current consumption requirement of the dedicated controller.

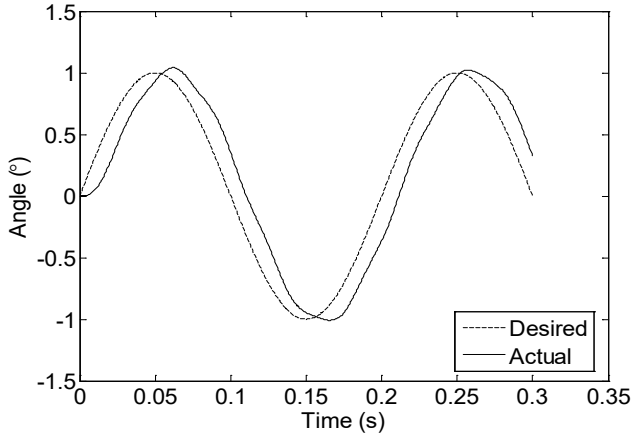

Figure 7:
Change of the fin angular position for δ_{f0}=1 ° with the PID type FLS controller

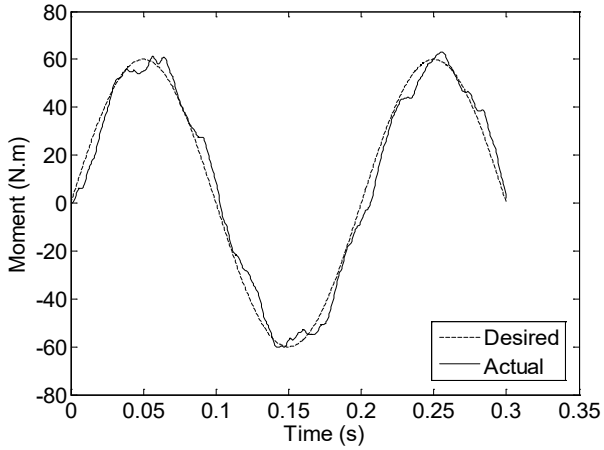

Figure 8:
Change of the hinge moment for δ_{f0}=1° with the PID type FLS controller

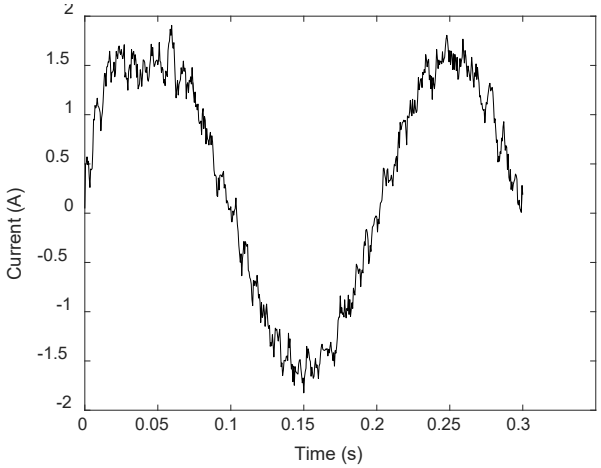

Figure 9:
Change of the current consumption for δ_{f0}=1° with the PID type FLS controller

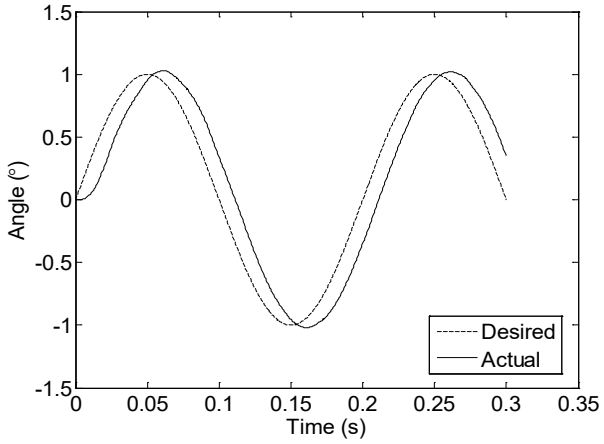

Figure 10:
Change of the fin angular position for δ_{f0}=1° with the H_∞ type FLS controller

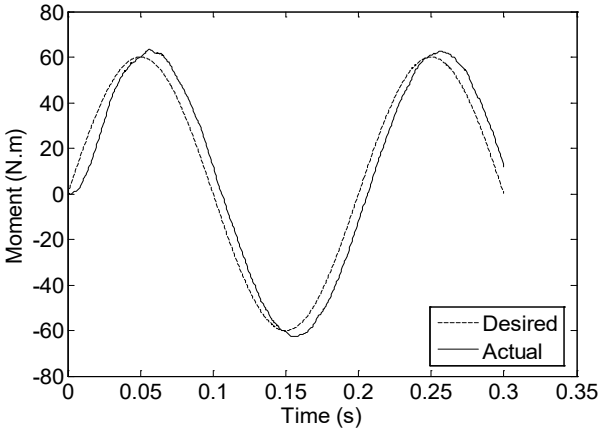

Figure 11:
Change of the hinge moment for $\delta_{f0}=1°$ with the H_∞ type FLS controller

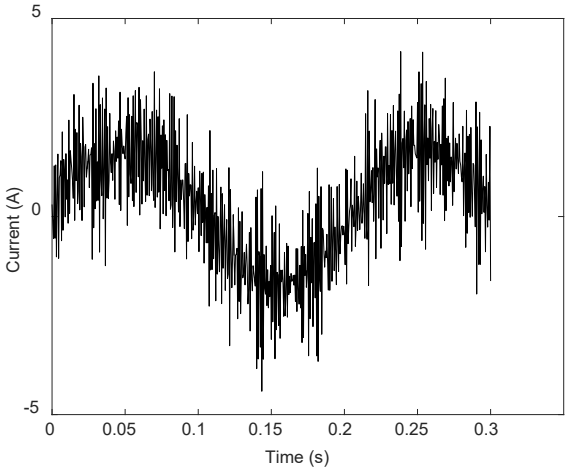

Figure 12:
Change of the current consumption for $\delta_{f0}=1°$ with the H_∞ type FLS controller

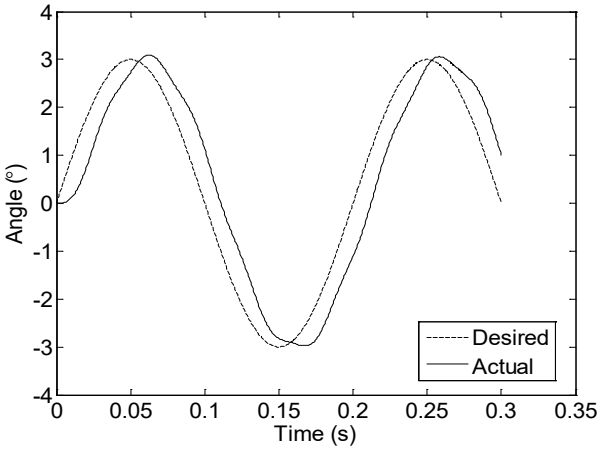

Figure 13:
Change of the fin angular position for $\delta_{f0}=3°$ with the PID type FLS controller

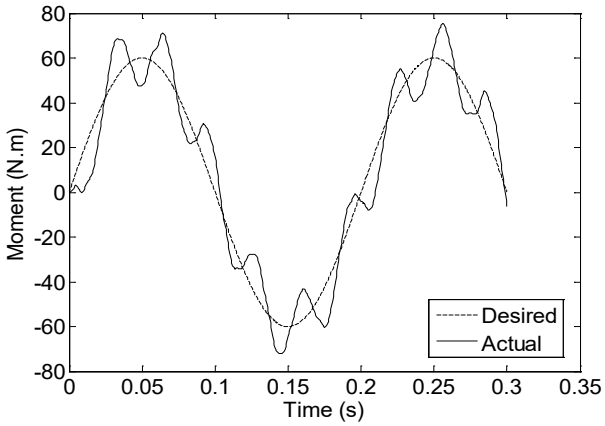

Figure 14:
Change of the hinge moment for $\delta_{f0}=3°$ with the PID type FLS controller

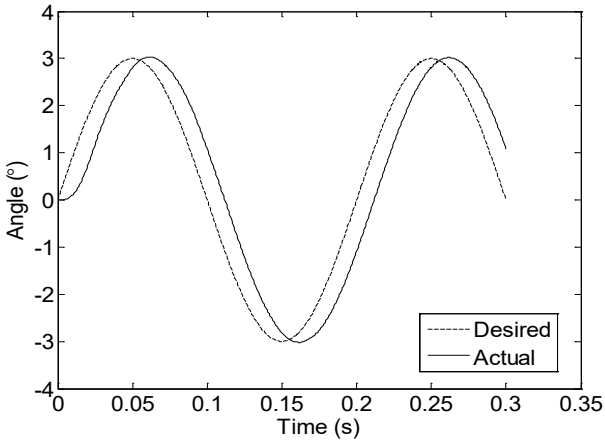

Figure 15:
Change of the fin angular position for $\delta_{f0}=3°$ with the H_∞ type FLS controller

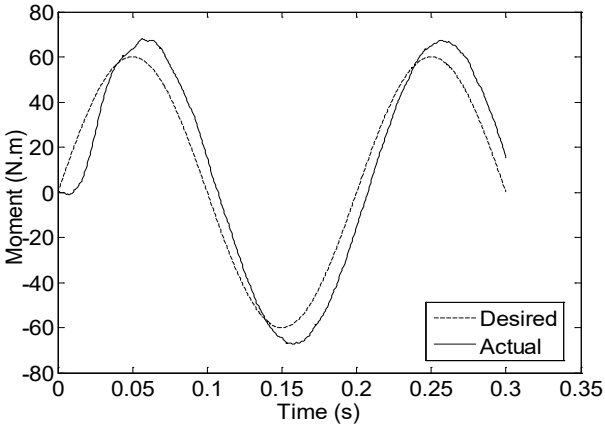

Figure 16:
Change of the hinge moment for $\delta_{f0}=3°$ with the H_∞ type FLS controller

Table 2. Results of the computer simulations

	Amplitude of the Fin Angular Position (δ_{f0}) (°)			
	1		3	
	PID Controller	H_∞ Controller	PID Controller	H_∞ Controller
Moment Error (N·m)	5.00	4.50	15.00	6.00
Angular Error (°)	0.10	0.08	0.20	0.15
Maximum Current Consumption (A)	1.91	4.16	2.49	4.52

5. DISCUSSION AND CONCLUSION

When the graphs in Figure 7 through Figure 14 are examined, it is seen that the response of the H_∞ type torque control system is better than the response of the FLS with the PID type controller. As the maximum amplitude of the fin angular position is increased from 1 to 3°, the mentioned difference becomes much clearer for the proposed control systems. Conversely, the current consumption of the H_∞-based control system happens to be larger than its PID-type counterpart. Namely, it reaches approximately 4.16 A for the configuration with the H_∞ type control system compared to the 1.91 A of peak consumption for the PID type control fort he fin angular position of 1°. On the other hand, this increment does not make any problem because the maximum current values occurring in the simulations are below the specified current threshold of the FLS motor.

Since the PID type controller can not handle the disturbing moment caused by the fin deflection, the resulting hinge moment values oscillate around the sinusoidal desired hinge moment. As shown in Figure 8 and Figure 12, these deviations may result in fatique on the fin connection rod.

If noticed, the magnitude of the fin deflections which are taken to be external disturbances on the FLS are kept at 1° maximum with an excitation frequency of 3 Hz. This is because the maximum amplitude of the fin deflections becomes smaller as the allowable deviation from the ideal (desired) system is lowered. If the fin deflection values are desired to be larger without losing the deviation tolerance, the gamma value of the designed H_∞ control system happens to be greater than 1. In fact, this causes the resulting control system to run in a degraded mode.

Evaluating the results of the conducted computer simulations, it is observed that the H_∞-based control system yields better performance than the PID-action-based classical control system. This judgement can be supplemented by the calculation of integral square error (ISE) parameter for both of the control cases (Kassem et al., 2017). Namely, regarding the δ_{f0}=1° case, the ISE values are obtained as 57,600 and 37,864 $(N\cdot m)^2\cdot s$ for PID and H_∞ control types, respectively. These quantities are turned into 129,600 and 69,696 $(N\cdot m)^2\cdot s$ for δ_{f0}=1°. As per the relevant experience, the improvement on the performance of the classical control systems becomes not better than that of the robust control systems especially for the present application. On the other hand, the design process of the robust control system needs some trade-off between the performance specifications and allowable limits on the system parameters.

ÇIKAR ÇATIŞMASI

Yazar, bilinen herhangi bir çıkar çatışması veya herhangi bir kurum/kuruluş ya da kişi ile ortak çıkar bulunmadığını onaylamaktadır.

YAZAR KATKISI

Bülent ÖZKAN, aşağıda sıralanan kriterlerin tamamına bu makale kapsamında katkıda bulunan tek yazardır:

i. Çalışmanın Kavramsal ve Tasarım Süreçlerinin Belirlenmesi
ii. Çalışmanın Kavramsal ve Tasarım Süreçlerinin Yönetimi
iii. Veri Toplama
iv. Veri Analizi ve Yorumlama
v. Makale Taslağının Oluşturulması
vi. Fikirsel İçeriğin Eleştirel İncelemesi
vii. Son Onay ve Tam Sorumluluk

REFERENCES

1. Arulmozhiyal, R., Murali, M. and Manikanadan, R. (2015) Modeling and simulation of control actuation system, *ARPN Journal of Engineering and Applied Sciences*, 10 (4), 1778-1782.

2. Blasi, L., Borrelli, M., D'Amato, E., di Grazia, L. E., Mattei, M. and Notaro, I. (2021) Modeling and control of a modular iron bird, *Aerospace*, 8(2), 39. doi: 10.3390/aerospace8020039

3. Borrelli, M., D'Amato, E., Emanuel di Grazia, L., Mattei, M. and Notaro, I. (2020). MPC load control for aircraft actuator testing, *2020 7th International Conference on Control, Decision and Information Technologies (CoDIT)*, Prague, Czech Republic.

4. https://www.ideal-aerosmith.com/ideal-product/aeroload-simulation-system, Date of access: 25.05.2022, Subject: *Aerodynamic Loading System*.

5. Jing, C. H., Xu, H. G. and Jiang, J. H. (2019). Dynamic surface disturbance rejection control for electro-hydraulic load simulator, *Mech. Syst. Signal. Process.* 134.

6. Kassem, A. M., Sayed, K., El-Zohri, E. H. and Ali, H. H. (2017) An integral square error-based model predictive controller for two area load frequency control, *Advances in Energy Research*, 5(1), 79-90. doi: 10.12989/eri.2017.5.1.079

7. Low K. H., Wang, H. and Wang M. Y. (2005) On the development of a real time control system by using xPC target: Solution to robotic system control, *2005 IEEE International Conference on Automation Science and Engineering*, Edmonton, Canada, 345-350.

8. Maekawa, H. (1999) Compact servo driver for torque control of DC-servo motor based on voltage control, *1999 IEEE/ASME International Conference on Advanced Intelligent Mechatronics*, Atlanta, USA, 341-346.

9. Muniraj, M. and Arulmozhiyal, R. (2015) Modeling and simulation of control actuation system with fuzzy-PID logic conrolled brushless motor drives for missiles glider applications, *The Scientific World Journal*, Hindawi Publishing Corporation, 1-11. doi: 10.1155/2015/723298

10. Nam, Y., Lee, J. and Sung K. H. (2000) Force control system design for aerodynamic load simulator, *American Control Conference*, Chicago, Illinois, USA, 3043-3046.

11. Ogata K. (1997) *Modern Control Engineering*, Third Edition, Prentice-Hall, USA.

12. Özkan B. (2005) *Dynamic Modeling, Guidance and Control of Homing Missiles*, PhD Thesis, Mechanical Engineering Department, Middle East Technical University, Ankara, Turkey.

13. Özkan, B. (2017) Dynamic modeling and control of a hydraulic fin loading system using ıntegral backstepping method, *Dokuz Eylül University, Faculty of Engineering Journal of Science and Engineering,* 19-56. doi: 10.21205/deufmd.2017195636

14. Özkan B., Yıldız E. N. and Dönmez B. (2008) Precise position control of a gimbaled camera system, *AIAA Guidance, Navigation, and Control Conference and Exhibit*, Honolulu, Hawaii, USA.

15. Özakalın, M. U., Salamci, M. U. and Özkan, B. (2014) Implementation of the sliding mode control with constant and varying sliding surfaces to a hydraulically-actuated fin loading system, *19th IFAC World Congress*, Cape Town, South Africa.

16. Page J. L. and Willis K. E. (1998) Designing motion systems for hardware-in-the-loop simulation, *Carco Electronics Publications*, USA.

17. Tekin, R. and Şahin, M. (2008) Development of a test device fort he loading tests of a missile control actuation system (in Turkish), *SAVTEK 2008-Defense Technologies Conference*, 601-607, Middle East Technical University, Ankara, Turkey.